Mathematical Biosciences and Engineering

MBE, 21(1): 1203–1227.
DOI: 10.3934/mbe.2024051
Received: 07 September 2023
Revised: 15 December 2023
Accepted: 20 December 2023
Published: 25 December 2023

http://www.aimspress.com/journal/MBE

Research article

Nonlinear extended state observer based control for the teleoperation of robotic systems with flexible joints

Yongli Yan[1], Fucai Liu[2], Teng Ren[3] and Li Ding[1,4,*]

[1] Beijing Advanced Innovation Center for Biomedical Engineering, Beihang University, Beijing 100083, China
[2] The Institute of Electrical Engineering, Yanshan University, Qinhuangdao 066004, China
[3] School of Mechanical Engineering, Shenyang University of Technology, Shenyang 110870, China
[4] School of Biological Science and Medical Engineering, Beihang University, Beijing 100083, China

* **Correspondence:** Email: ding1971316@buaa.edu.cn.

Abstract: The control of robot manipulator pose is significantly complicated by the uncertainties arising from flexible joints, presenting substantial challenges in incorporating practical operational constraints. These challenges are further exacerbated in teleoperation scenarios, where factors such as synchronization and external disturbances further amplify the difficulties. At the core of this research is the introduction of a pioneering teleoperation controller, ingeniously integrating a nonlinear extended state observer (ESO) with the barrier Lyapunov function (BLF) while effectively accommodating a steady time delay. The controller in our study demonstrates exceptional proficiency in accurately estimating uncertainties arising from both flexible joints and external disturbances using the nonlinear ESO. Refined estimates, in conjunction with operational constraints of the system, are integrated into our BLF-based controller. Consequently, a synchronized control mechanism for teleoperation is achieved, exhibiting promising performance. Importantly, our experimental findings provide substantial evidence that our proposed approach effectively reduces the tracking error of the teleoperation system to within 0.02 rad. This advancement highlights the potential of our controller in significantly enhancing the precision and reliability of teleoperated robot manipulators.

Keywords: nonlinear extended state observer; teleoperation; flexible joints; barrier Lyapunov function; state constraint

Nomenclature

$(\bullet)_{\mathrm{m}},(\bullet)_{\mathrm{s}}$	Subscripts $\{m,\ s\}$ denote the master robot and the slave robot, respectively.
$(\hat{\bullet})$	Diacritical mark wedge denotes the estimation, for example, $\hat{\Theta}$ is the estimation of Θ.
$(\tilde{\bullet})$	Diacritical mark tilde denotes the estimation error, for example $\tilde{\Theta}=\Theta-\hat{\Theta}$.
$q_i,\dot{q}_i,\ddot{q}_i$	n-dimensional joint position, velocity, acceleration, $i = m,\ s$.
$M_i(q_i)$	Robotic inertia matrix, $i = m,\ s$.
$C_i(q_i,\dot{q}_i)$	Coriolis/centrifugal matrix, $i = m,\ s$.
$f_i(q_i)$	Viscous friction force vector, $i = m,\ s$.
$B_i(q_i)$	Bounded external disturbance, $i = m,\ s$.
$G_i(q_i)$	Gravity torque, $i = m,\ s$.
τ_i	Control torque, $i = m,\ s$.
$\tau_{\mathrm{h}},\tau_{\mathrm{e}}$	Forces exerted on the end-effectors of the master and slave robots by the human operator and environment, respectively.
$\theta_i,\dot{\theta}_i,\ddot{\theta}_i$	n-dimensional angular position, velocity, acceleration, $i = m,\ s$.
J_{s}	Jacobian matrix of the slave robot.
τ_{f}	Friction caused by the motor shaft, where the subscript {f} represents variables associated with friction caused by the motor shaft.
τ_{c}	Torque generated by the flexibility of the joint, where the subscript {c} represents variables associated with the joint.
K_{s}	Equivalent stiffness coefficient of the joint in the slave robot.
$R^n,R^{n\times m}$	n-dimensional real space and $n \times m$ dimensional real matrix space, respectively.
T_i	Communication delays, $i = m,\ s$.
Z_{ik}	State variable of ESO, $i = m,\ s,\ k = 1,2,3$.
e_{ik}	State estimation error of ESO, $i = m,\ s,\ k = 1,2,3$.

1. Introduction

The implementation of teleoperation within robotic systems extends the ability of humans to perform specific operations personally in remote environments. Teleoperation is conducted by remote operators transmitting control signals to robotic systems through communication channels, and receiving the force interaction data from the robotic system via the same communication channels. Currently, teleoperation systems find extensive applications in diverse fields including remote surgery and deep-sea exploration [1–3].

Increasing interest has been generated in recent years for developing robotic systems with flexible manipulator joints. This is mainly due to two reasons [4,5]. First, the increasing complexity and refinement of industrial tasks has necessitated the implementation of elastic drive transmission systems in industrial robots, such as harmonic gear transmission, joint torque sensors, and belt pulleys [6]. These must be treated as flexible-joint systems to mitigate the negative impact of end effector vibrations on system stability [7]. Second, flexible components have been introduced in new robotic manipulator designs for obtaining more human-compatible mobility characteristics that facilitate human-robot interactions, such as high flexibility, strong adaptability, and strong robustness [8]. However, the flexibility of these joints renders the dynamic behavior of robotic systems increasingly intricate and challenging to model. This complexity primarily stems from nonlinearity, uncertainty, damping effects, and vibration modes of flexible joints, presenting a significant challenge in achieving satisfactory control performance in remote operation systems.

Since Spong proposed the flexible joint model in 1987, more and more control strategies have been proposed for manipulator systems with flexible joints [9]. Spong [10], Ghorbel et al. [11], and Chang and Daniel [12] designed an adaptive controller based on singular perturbation control. However, although this method can simplify the analysis, it may also oversimplify the system dynamics, potentially ignoring the key nonlinearity and complexity existing in the real scene [13]. Nam et al. [14] introduced finite time control based on sliding mode control and designed a control strategy that enables a flexible joint manipulator system to achieve effective tracking. However, the presence of buffeting reduces the tracking effect of the system. In addition, backstepping control is also a highly effective control strategy for addressing the tracking control problem in flexible joint manipulator systems. There have been many research achievements based on backstepping to solve control issues in flexible manipulator systems. Huang et al. [15] designed the controller of the single-link flexible manipulator system based on the reverse step method, but this control strategy is only applicable to a system with known state parameters. Cheng et al. [16] combined the singular perturbation control method and adaptive control method on the basis of backstep method to design a control strategy suitable for a flexible manipulator system. However, this control strategy has the disadvantage of too having complicated of a calculation. To tackle this issue, Sahu et al. [17] proposed a backstepping control strategy that combines extended state observer (ESO) with backstepping control. This approach not only effectively addresses the computational complexity in traditional backstepping but also efficiently handles the uncertainty and interference of the internal model, significantly improving the tracking performance of the system.

ESO is a part of active disturbance rejection control (ADRC) theory that enables real-time estimation of internal state and unmodeled dynamics of a system [18,19]. Recently, ESO has been widely applied, such as in tracked vehicle control [20], quadrotor control [21], DC-link voltage control [22], and permanent magnet synchronous linear motor (PMSLM) servo system control [23]. ESO can be

categorized into linear and nonlinear types. Linear ESO can exhibit peaking phenomena when dealing with nonlinearities and strong couplings, thereby potentially compromising the observer's accuracy to some extent [24]. Consequently, in this study, nonlinear ESO was chosen to address the uncertainty in the internal model and external disturbances of the flexible-joint teleoperation system, enhancing its robustness and accuracy.

Furthermore, in real-world engineering applications, the system may face limitations due to factors such as temperature and space. If the system's operation exceeds predefined boundaries, it can adversely affect the system's performance and, in extreme cases, potentially lead to system failures, endangering the personal safety of the operators. The barrier Lyapunov function (BLF) is a standard method developed for implementing constrained control problems of this nature [25]. Wang [26] and Li et al. [27] used the barrier Lyapunov function to ensure that the input and output of a nonlinear system are controlled within a preset interval. Using the above research results, Zhang [28] and Yu et al. [29] applied the barrier Lyapunov function to a robot arm system with limited output, and ensured that the output of the system could be controlled within a preset interval.

While considerable progress has been made in the control of robotic systems with flexible joints, these developments have been rarely applied in the design of teleoperation systems for remote robotic control. Moreover, teleoperation systems not only must address the many uncertainties in the pose control of robotic manipulators, but also account for complexities in the actual working environments, and the inevitability of external interference. Accordingly, these issues remain poorly addressed by the current state of teleoperation system development.

In summary, to achieve effective tracking of joint position trajectories for a state-constrained flexible-joint teleoperation system, this paper proposes a control strategy based on the combination of nonlinear ESO and the Barrier Lyapunov Function. The main contributions in this work are summarized as follows: 1) The paper introduces a novel teleoperation controller that employs a nonlinear Extended State Observer (ESO) to estimate internal uncertainties related to flexible joints and external disturbances. This inclusion enhances the accuracy of the control system by actively predicting and compensating for disturbances in the input channel. 2) The research effectively addresses practical operational constraints on the system output states by leveraging the Barrier Lyapunov Function (BLF). This application ensures that the teleoperation controller operates within defined limitations, leading to more reliable and controlled system behavior. 3) The study focuses on a robotic system that combines a rigid master manipulator and a flexible slave manipulator. By enforcing constraints on the system output states using the BLF, synchronized control is achieved between these two distinct components. This synchronization is critical for precise and coordinated control in teleoperation scenarios.

The remainder of this paper is organized as follows: Section 2 presents the pertinent preliminary discussion. Section 3 elucidates the nonlinear ESO and stability analyses of the proposed teleoperation control system. Following this, Section 4 provides a detailed account of the experimental results. Finally, concluding remarks and future directions are outlined in Section 5.

2. Preliminary discussion

The rigid master manipulator is assumed to have n degrees of freedom, and its nonlinear dynamic behavior is defined as follows.

$$M_{\mathrm{m}}\left(q_{\mathrm{m}}\right)\ddot{q}_{\mathrm{m}}+C_{\mathrm{m}}\left(q_{\mathrm{m}},\dot{q}_{\mathrm{m}}\right)\dot{q}_{\mathrm{m}}+f_{\mathrm{m}}\left(q_{\mathrm{m}}\right)+B_{\mathrm{m}}\left(q_{\mathrm{m}}\right)+G_{\mathrm{m}}\left(q_{\mathrm{m}}\right)=\tau_{\mathrm{m}}+\tau_{\mathrm{h}} \tag{1}$$

Similarly, the flexible slave manipulator is assumed to have n degrees of freedom, and its nonlinear dynamic behavior is defined as follows [9].

$$\begin{cases} M_{\mathrm{s}}\left(q_{\mathrm{s}}\right)\ddot{q}_{\mathrm{s}}+C_{\mathrm{s}}\left(q_{\mathrm{s}},\dot{q}_{\mathrm{s}}\right)\dot{q}_{\mathrm{s}}+f_{\mathrm{s}}\left(q_{\mathrm{s}}\right)+B_{\mathrm{s}}\left(q_{\mathrm{s}}\right)+G_{\mathrm{s}}\left(q_{\mathrm{s}}\right)=\tau_{\mathrm{c}}-\tau_{\mathrm{e}} \\ J_{\mathrm{s}}\ddot{\theta}_{\mathrm{s}}+\tau_{\mathrm{c}}=\tau_{\mathrm{s}}+\tau_{\mathrm{f}} \end{cases} \tag{2}$$

Here, for all $i=\mathrm{m},\mathrm{s}$, $q_i\in R^n$, $M_i\left(q_i\right)\in R^{n\times n}$, $C_i\left(\dot{q}_i,q_i\right)\in R^{n\times n}$, $f_i\left(q_i\right)\in R^n$, $B_i\left(q_i\right)\in R^n$, $G_i\left(q_i\right)\in R^n$, $J_{\mathrm{s}}\in R^{n\times n}$, $\theta_{\mathrm{s}}\in R^n$, $\tau_i\in R^n$, $\tau_{\mathrm{c}}\in R^n$, $\tau_{\mathrm{h}}\in R^n$, $\tau_{\mathrm{e}}\in R^n$, $\tau_{\mathrm{f}}\in R^n$, $\tau_{\mathrm{c}}=K_{\mathrm{s}}\left(\theta_{\mathrm{s}}-q_{\mathrm{s}}\right)$, $\mathrm{K}_{\mathrm{s}}\in R^{n\times n}$.

For convenience, we make the following substitutions in the system variables: $X_{\mathrm{m1}}=q_{\mathrm{m}}$, $X_{\mathrm{m2}}=\dot{q}_{\mathrm{m}}$, $X_{\mathrm{s1}}=q_{\mathrm{s}}$, $X_{\mathrm{s2}}=\dot{q}_{\mathrm{s}}$, $X_{\mathrm{s3}}=\theta_{\mathrm{s}}$, and $X_{\mathrm{s4}}=\dot{\theta}_{\mathrm{s}}$. Then, the following correspondences are applied.

$$\begin{cases} \dot{X}_{\mathrm{m1}}=X_{\mathrm{m2}} \\ \dot{X}_{\mathrm{m2}}=F_{\mathrm{m}}+M_{\mathrm{m}}^{-1}\tau_{\mathrm{m}} \end{cases} \tag{3}$$

$$\begin{cases} \dot{X}_{\mathrm{s1}}=X_{\mathrm{s2}} \\ \dot{X}_{\mathrm{s2}}=F_{\mathrm{s}}+M_{\mathrm{s}}^{-1}\tau_{\mathrm{c}} \\ \dot{X}_{\mathrm{s3}}=X_{\mathrm{s4}} \\ \dot{X}_{\mathrm{s4}}=F_{\mathrm{f}}+J_{\mathrm{s}}^{-1}\tau_{\mathrm{s}} \end{cases} \tag{4}$$

The variables F_{m}, F_{s}, and F_{f} in (3) and (4) represent lumped uncertainties in the system, which contain internal uncertain parts and external perturbations, which are defined as follows.

$$\begin{cases} F_{\mathrm{m}}=-M_{\mathrm{m}}^{-1}\left(C_{\mathrm{m}}X_{\mathrm{m2}}+f_{\mathrm{m}}\left(X_{\mathrm{m1}}\right)+B_{\mathrm{m}}\left(X_{\mathrm{m1}}\right)+G_{\mathrm{m}}\left(X_{\mathrm{m1}}\right)-\tau_{\mathrm{h}}\right) \\ F_{\mathrm{s}}=-M_{\mathrm{s}}^{-1}\left(C_{\mathrm{s}}X_{\mathrm{s2}}+f_{\mathrm{s}}\left(X_{\mathrm{s1}}\right)+B_{\mathrm{s}}\left(X_{\mathrm{s1}}\right)+G_{\mathrm{s}}\left(X_{\mathrm{s1}}\right)+\tau_{\mathrm{e}}\right) \\ F_{\mathrm{f}}=J_{\mathrm{s}}^{-1}\left(\tau_{\mathrm{f}}-\tau_{\mathrm{c}}\right) \end{cases} \tag{5}$$

By treating uncertainties such as τ_{c} as total perturbations, the design of the control system can be simplified, resulting in reduced computational load. This approach enhances the system's robustness to various disturbances while maintaining the effectiveness and flexibility of the control strategy.

3. Controller design and stability analysis

3.1. Nonlinear ESO design

The nonlinear ESO is applied for estimating the interference terms F_m and F_s. In this subsection, we design the observer for F_m only, and subsequently analyze its error estimation stability. The F_s and F_f estimator design and stability are entirely equivalent and are therefore not presented herein.

First, the nonlinear ESO is designed by introducing the following expansion terms:

$$\begin{cases} X_{m3} = F_m \\ \dot{X}_{m3} = -h_m \end{cases} \tag{6}$$

where h_m denotes the derivative of external disturbances. Before designing the ESO, the following assumption about external disturbances is given in this paper.

Assumption 1: For the external disturbance in the nonlinear bilateral teleoperation system, there exists a positive unknown constant L such that $\left|h_{\mathrm{m}}\right| \le L$ holds.

We define the estimation error as

$$e_{\mathrm{m}k} = Z_{\mathrm{m}k} - X_{\mathrm{m}k},\ k = 1,2,3, \tag{7}$$

where Z_{m1}, Z_{m2}, and Z_{m3} are the estimated values of X_{m1}, X_{m2}, and X_{m3}, respectively, and introduce new parametric variables

$$\eta_{\mathrm{m}k} = \frac{e_{\mathrm{m}k}}{\varepsilon^{3-k}},\ k = 1,2,3, \tag{8}$$

where ε is an appropriate positive definite parameter. Then, the nonlinear ESO is designed in the following form:

$$\begin{cases} \dot{Z}_{\mathrm{m1}} = Z_{\mathrm{m2}} - \beta_{\mathrm{m1}}\varepsilon\left|\eta_{\mathrm{m1}}\right|^{\frac{3}{2}}\operatorname{sgn}\left(\eta_{\mathrm{m1}}\right) \\ \dot{Z}_{\mathrm{m2}} = Z_{\mathrm{m3}} - \beta_{\mathrm{m2}}\left|\eta_{\mathrm{m1}}\right|^{\frac{1}{2}}\operatorname{sgn}\left(\eta_{\mathrm{m1}}\right) + M_{\mathrm{m}}^{-1}\tau_{\mathrm{m}} \\ \dot{Z}_{\mathrm{m3}} = -\beta_{\mathrm{m3}}\varepsilon^{-1}\operatorname{sgn}\left(\eta_{\mathrm{m1}}\right) \end{cases} \tag{9}$$

Here, sgn(·) is the signum function that returns the sign of its argument, and β_{m1}, β_{m2}, and β_{m3} are appropriate positive definite parameters. Combining Eqs (6)–(9), the estimation error of the system can be obtained as follows.

$$\begin{cases} \dot{e}_{\mathrm{m}1} = e_{\mathrm{m}2} - \beta_{\mathrm{m}1}\varepsilon\left|\eta_{\mathrm{m}1}\right|^{\frac{3}{2}}\operatorname{sgn}\left(\eta_{\mathrm{m}1}\right) \\ \dot{e}_{\mathrm{m}2} = e_{\mathrm{m}3} - \beta_{\mathrm{m}2}\left|\eta_{\mathrm{m}1}\right|^{\frac{1}{2}}\operatorname{sgn}\left(\eta_{\mathrm{m}1}\right) \\ \dot{e}_{\mathrm{m}3} = h_{\mathrm{m}} - \beta_{\mathrm{m}3}\varepsilon^{-1}\operatorname{sgn}\left(\eta_{\mathrm{m}1}\right) \end{cases} \tag{10}$$

Finally, both sides of the three expressions in error system (10) are multiplied from top to bottom by $\frac{1}{\varepsilon}$, 1, and ε, respectively, which yields the substitution of error system (10) as follows:

$$\begin{cases} \varepsilon\dot{\eta}_{\mathrm{m}1} = \eta_{\mathrm{m}2} - \beta_{\mathrm{m}1}\left|\eta_{\mathrm{m}1}\right|^{\frac{3}{2}}\operatorname{sgn}\left(\eta_{\mathrm{m}1}\right) \\ \varepsilon\dot{\eta}_{\mathrm{m}2} = \eta_{\mathrm{m}3} - \beta_{\mathrm{m}2}\left|\eta_{\mathrm{m}1}\right|^{\frac{1}{2}}\operatorname{sgn}\left(\eta_{\mathrm{m}1}\right) \\ \varepsilon\dot{\eta}_{\mathrm{m}3} = \varepsilon h_{\mathrm{m}} - \beta_{\mathrm{m}3}\operatorname{sgn}\left(\eta_{\mathrm{m}1}\right) \end{cases} \tag{11}$$

Theorem 1: *For master manipulator system (1) and nonlinear error system (11), the estimation error* $e_{\mathrm{m}k}\left(k=1,2,3\right)$ *will converge to the neighborhood of the origin if there exist positive definite parameters* $\beta_{\mathrm{m}1}$, $\beta_{\mathrm{m}2}$, *and* $\beta_{\mathrm{m}3}$ *such that the following inequality is guaranteed.*

$$Q = \begin{bmatrix} -\frac{1}{\varepsilon}k_8\beta_{\mathrm{m}1} & \frac{1}{\varepsilon}k_1 & \frac{1}{\varepsilon}k_4 & 0 \\ * & -\left(\frac{1}{\varepsilon}k_4 - k_9^2 - k_6^2\right) & \frac{1}{\varepsilon}k_5 + \frac{1}{\varepsilon}k_2 & \frac{1}{\varepsilon}\left(k_7 + k_4\beta_{\mathrm{m}1}\right) \\ * & * & -\left(\frac{1}{\varepsilon}k_6 - k_3^2\right) & -\frac{1}{\varepsilon}k_5\beta_{\mathrm{m}1} \\ * & * & * & -\frac{1}{\varepsilon}k_7\beta_{\mathrm{m}1} \\ * & * & * & * \\ * & * & * & * \\ * & * & * & * \end{bmatrix}$$

$$\begin{bmatrix} 0 & 0 & 0 \\ 0 & 0 & \frac{1}{\varepsilon}\left(k_8 - k_2\beta_{\mathrm{m}2}\right) \\ 0 & 0 & \frac{1}{\varepsilon}k_6\beta_{\mathrm{m}2} \\ 0 & 0 & 0 \\ -\frac{1}{\varepsilon}k_1\beta_{\mathrm{m}1} & 0 & 0 \\ * & -\frac{1}{\varepsilon}\left(k_9\beta_{\mathrm{m}1} - k_4\beta_{\mathrm{m}2}\right) & 0 \\ * & * & -k_9 - \frac{1}{\varepsilon}\beta_{\mathrm{m}3} \end{bmatrix} \le 0 \tag{12}$$

where $k_1 - k_9$ *are appropriate positive definite constants and the following inequality group holds:*

$$\begin{cases} k_1 - k_4 - k_5 \ge 0 \\ k_2 - k_4 - k_6 \ge 0 \\ k_3 - k_5 - k_6 \ge 0 \end{cases} \tag{13}$$

Proof: The proof is based on the following Lyapunov function:

$$\begin{aligned} V = {} & \frac{1}{2}k_1\eta_{\mathrm{m}1}^2 + \frac{1}{2}k_2\eta_{\mathrm{m}2}^2 + \frac{1}{2}k_3\eta_{\mathrm{m}3}^2 - k_4\eta_{\mathrm{m}1}\eta_{\mathrm{m}2} + k_5\eta_{\mathrm{m}1}\eta_{\mathrm{m}3} - k_6\eta_{\mathrm{m}2}\eta_{\mathrm{m}3} \\ & + \frac{2}{5}k_7\left|\eta_{\mathrm{m}1}\right|^{\frac{5}{2}} + \frac{2}{3}k_8\left|\eta_{\mathrm{m}1}\right|^{\frac{3}{2}} + k_9\left|\eta_{\mathrm{m}1}\right| \end{aligned} \tag{14}$$

From Young's inequality, the following inequality group can be obtained:

$$\begin{cases} k_4\eta_{\mathrm{m}1}\eta_{\mathrm{m}2} \le \frac{k_4}{2}\left(\eta_{\mathrm{m}1}^2 + \eta_{\mathrm{m}2}^2\right) \\ -k_5\eta_{\mathrm{m}1}\eta_{\mathrm{m}3} \le \frac{k_5}{2}\left(\eta_{\mathrm{m}1}^2 + \eta_{\mathrm{m}3}^2\right) \\ k_6\eta_{\mathrm{m}2}\eta_{\mathrm{m}3} \le \frac{k_6}{2}\left(\eta_{\mathrm{m}2}^2 + \eta_{\mathrm{m}3}^2\right) \end{cases} \tag{15}$$

Substituting Eq (15) into Eq (14), the following inequality can be obtained:

$$\begin{aligned} V \ge {} & \frac{1}{2}\left(k_1 - k_4 - k_5\right)\eta_{\mathrm{m}1}^2 + \frac{1}{2}\left(k_2 - k_4 - k_6\right)\eta_{\mathrm{m}2}^2 + \frac{1}{2}\left(k_3 - k_5 - k_6\right)\eta_{\mathrm{m}3}^2 \\ & + \frac{2}{5}k_7\left|\eta_{\mathrm{m}1}\right|^{\frac{5}{2}} + \frac{2}{3}k_8\left|\eta_{\mathrm{m}1}\right|^{\frac{3}{2}} + k_9\left|\eta_{\mathrm{m}1}\right| \end{aligned} \tag{16}$$

When positive definite constants k_1–k_9 satisfy inequality group (13), the Lyapunov function (14) is positive semidefinite.

From the converted error system (11), taking the derivative of (14) with respect to time yields the following:

$$\begin{aligned}\dot{V} &= k_1\eta_{\mathrm{m1}}\dot{\eta}_{\mathrm{m1}} + k_2\eta_{\mathrm{m2}}\dot{\eta}_{\mathrm{m2}} + k_3\eta_{\mathrm{m3}}\dot{\eta}_{\mathrm{m3}} - k_4\dot{\eta}_{\mathrm{m1}}\eta_{\mathrm{m2}} - k_4\eta_{\mathrm{m1}}\dot{\eta}_{\mathrm{m2}} \\ &\quad + k_5\dot{\eta}_{\mathrm{m1}}\eta_{\mathrm{m3}} + k_5\eta_{\mathrm{m1}}\dot{\eta}_{\mathrm{m3}} - k_6\dot{\eta}_{\mathrm{m2}}\eta_{\mathrm{m3}} - k_6\eta_{\mathrm{m2}}\dot{\eta}_{\mathrm{m3}} \\ &\quad + k_7\left|\eta_{\mathrm{m1}}\right|^{\frac{3}{2}}\operatorname{sgn}\left(\eta_{\mathrm{m1}}\right)\dot{\eta}_{\mathrm{m1}} + k_8\left|\eta_{\mathrm{m1}}\right|^{\frac{1}{2}}\operatorname{sgn}\left(\eta_{\mathrm{m1}}\right)\dot{\eta}_{\mathrm{m1}} + k_9\operatorname{sgn}\left(\eta_{\mathrm{m1}}\right)\dot{\eta}_{\mathrm{m1}}\end{aligned} \tag{17}$$

According to error system (11), we can reconfigure (17) as follows:

$$\begin{aligned}\dot{V} &= \left[k_1\eta_{\mathrm{m1}} - k_4\eta_{\mathrm{m2}} + k_5\eta_{\mathrm{m3}} + k_7\left|\eta_{\mathrm{m1}}\right|^{\frac{3}{2}}\operatorname{sgn}\left(\eta_{\mathrm{m1}}\right) + k_8\left|\eta_{\mathrm{m1}}\right|^{\frac{1}{2}}\operatorname{sgn}\left(\eta_{\mathrm{m1}}\right) + k_9\operatorname{sgn}\left(\eta_{\mathrm{m1}}\right)\right] \\ &\quad \frac{1}{\varepsilon}\left[\eta_{\mathrm{m2}} - \beta_{\mathrm{m1}}\left|\eta_{\mathrm{m1}}\right|^{\frac{3}{2}}\operatorname{sgn}\left(\eta_{\mathrm{m1}}\right)\right] \\ &\quad + \left[k_2\eta_{\mathrm{m2}} - k_4\eta_{\mathrm{m1}} - k_6\eta_{\mathrm{m3}}\right]\frac{1}{\varepsilon}\left[\eta_{\mathrm{m3}} - \beta_{\mathrm{m2}}\left|\eta_{\mathrm{m1}}\right|^{\frac{1}{2}}\operatorname{sgn}\left(\eta_{\mathrm{m1}}\right)\right] \\ &\quad + \left[k_3\eta_{\mathrm{m3}} + k_5\eta_{\mathrm{m1}} - k_6\eta_{\mathrm{m2}}\right]\frac{1}{\varepsilon}\left[\varepsilon h_{\mathrm{m}} - \beta_{\mathrm{m3}}\operatorname{sgn}\left(\eta_{\mathrm{m1}}\right)\right]\end{aligned} \tag{18}$$

This is further expanded as follows:

$$\begin{aligned}\dot{V} &= \frac{1}{\varepsilon}k_1\eta_{\mathrm{m1}}\eta_{\mathrm{m2}} - \frac{1}{\varepsilon}k_4\eta_{\mathrm{m2}}^2 + \frac{1}{\varepsilon}k_5\eta_{\mathrm{m2}}\eta_{\mathrm{m3}} + k_7\left|\eta_{\mathrm{m1}}\right|^{\frac{3}{2}}\operatorname{sgn}\left(\eta_{\mathrm{m1}}\right)\eta_{\mathrm{m2}} \\ &\quad + \frac{1}{\varepsilon}k_8\left|\eta_{\mathrm{m1}}\right|^{\frac{1}{2}}\operatorname{sgn}\left(\eta_{\mathrm{m1}}\right)\eta_{\mathrm{m2}} + \frac{1}{\varepsilon}k_9\operatorname{sgn}\left(\eta_{\mathrm{m1}}\right)\eta_{\mathrm{m2}} - \frac{1}{\varepsilon}k_1\beta_{\mathrm{m1}}\left|\eta_{\mathrm{m1}}\right|^{\frac{5}{2}} \\ &\quad + \frac{1}{\varepsilon}k_4\beta_{\mathrm{m1}}\left|\eta_{\mathrm{m1}}\right|^{\frac{3}{2}}\operatorname{sgn}\left(\eta_{\mathrm{m1}}\right)\eta_{\mathrm{m2}} - \frac{1}{\varepsilon}k_5\beta_{\mathrm{m1}}\left|\eta_{\mathrm{m1}}\right|^{\frac{3}{2}}\operatorname{sgn}\left(\eta_{\mathrm{m1}}\right)\eta_{\mathrm{m3}} \\ &\quad - \frac{1}{\varepsilon}k_8\beta_{\mathrm{m1}}\eta_{\mathrm{m1}}^2 - \frac{1}{\varepsilon}k_9\beta_{\mathrm{m1}}\left|\eta_{\mathrm{m1}}\right|^{\frac{3}{2}} + \frac{1}{\varepsilon}k_2\eta_{\mathrm{m2}}\eta_{\mathrm{m3}} - \frac{1}{\varepsilon}k_4\eta_{\mathrm{m1}}\eta_{\mathrm{m3}} \\ &\quad - \frac{1}{\varepsilon}k_6\eta_{\mathrm{m3}}^2 - \frac{1}{\varepsilon}k_2\beta_{\mathrm{m2}}\left|\eta_{\mathrm{m1}}\right|^{\frac{1}{2}}\operatorname{sgn}\left(\eta_{\mathrm{m1}}\right)\eta_{\mathrm{m2}} + \frac{1}{\varepsilon}k_4\beta_{\mathrm{m2}}\left|\eta_{\mathrm{m1}}\right|^{\frac{3}{2}} - \frac{1}{\varepsilon}k_7\beta_{\mathrm{m1}}\left|\eta_{\mathrm{m1}}\right|^{3} \\ &\quad + \frac{1}{\varepsilon}k_6\beta_{\mathrm{m2}}\left|\eta_{\mathrm{m1}}\right|^{\frac{1}{2}}\operatorname{sgn}\left(\eta_{\mathrm{m1}}\right)\eta_{\mathrm{m3}} - \left(\frac{1}{\varepsilon}k_6\eta_{\mathrm{m2}} - \frac{1}{\varepsilon}k_3\eta_{\mathrm{m3}}\right)\left[\varepsilon h_{\mathrm{m}} - \beta_{\mathrm{m3}}\operatorname{sgn}\left(\eta_{\mathrm{m1}}\right)\right] \\ &\quad + \frac{1}{\varepsilon}k_5\eta_{\mathrm{m1}}\left[\varepsilon h_{\mathrm{m}} - \beta_{\mathrm{m3}}\operatorname{sgn}\left(\eta_{\mathrm{m1}}\right)\right]\end{aligned} \tag{19}$$

This can be transformed into the following inequality:

$$\begin{aligned}\dot{V} \le & -\frac{1}{\varepsilon}k_8\beta_{\mathrm{m1}}\eta_{\mathrm{m1}}^2-\left(\frac{1}{\varepsilon}k_4-k_9^2-k_6^2\right)\eta_{\mathrm{m2}}^2-\left(\frac{1}{\varepsilon}k_6-k_3^2\right)\eta_{\mathrm{m3}}^2\\ & +\frac{1}{\varepsilon}k_1\eta_{\mathrm{m1}}\eta_{\mathrm{m2}}+\left(\frac{1}{\varepsilon}k_2+\frac{1}{\varepsilon}k_5\right)\eta_{\mathrm{m2}}\eta_{\mathrm{m3}}-\frac{1}{\varepsilon}k_7\beta_{\mathrm{m1}}\left|\eta_{\mathrm{m1}}\right|^3-\frac{1}{\varepsilon}k_4\eta_{\mathrm{m1}}\eta_{\mathrm{m3}}\\ & -\frac{1}{\varepsilon}k_1\beta_{\mathrm{m1}}\left|\eta_{\mathrm{m1}}\right|^{\frac{5}{2}}-\left(\frac{1}{\varepsilon}k_9\beta_{\mathrm{m1}}-\frac{1}{\varepsilon}k_4\beta_{\mathrm{m2}}\right)\left|\eta_{\mathrm{m1}}\right|^{\frac{3}{2}}-\left(\frac{1}{\varepsilon}k_5\beta_{\mathrm{m3}}-k_5\right)\left|\eta_{\mathrm{m1}}\right|\\ & +\left(\frac{1}{\varepsilon}k_7+\frac{1}{\varepsilon}k_4\beta_{\mathrm{m1}}\right)\left|\eta_{\mathrm{m1}}\right|^{\frac{3}{2}}\mathrm{sgn}\left(\eta_{\mathrm{m1}}\right)\eta_{\mathrm{m2}}-\frac{1}{\varepsilon}k_5\beta_{\mathrm{m1}}\left|\eta_{\mathrm{m1}}\right|^{\frac{3}{2}}\mathrm{sgn}\left(\eta_{\mathrm{m1}}\right)\eta_{\mathrm{m3}}\\ & +\left(\frac{1}{\varepsilon}k_8-\frac{1}{\varepsilon}k_2\beta_{\mathrm{m2}}\right)\left|\eta_{\mathrm{m1}}\right|^{\frac{1}{2}}\mathrm{sgn}\left(\eta_{\mathrm{m1}}\right)\eta_{\mathrm{m2}}+\frac{1}{\varepsilon}k_6\beta_{\mathrm{m2}}\left|\eta_{\mathrm{m1}}\right|^{\frac{1}{2}}\mathrm{sgn}\left(\eta_{\mathrm{m1}}\right)\eta_{\mathrm{m3}}\\ & +\frac{1}{\varepsilon^2}\left[\varepsilon h_{\mathrm{m}}-\beta_{\mathrm{m3}}\,\mathrm{sgn}\left(\eta_{\mathrm{m1}}\right)\right]^2+\frac{1}{4\varepsilon^2}\end{aligned} \tag{20}$$

Therefore,

$$\dot{V} \le \xi\left(t\right)Q\xi^{\mathrm{T}}\left(t\right)+\frac{1}{\varepsilon^2}\left[\varepsilon h_{\mathrm{m}}-\beta_{\mathrm{m3}}\,\mathrm{sgn}\left(\eta_{\mathrm{m1}}\right)\right]^2+\frac{1}{4\varepsilon^2} \tag{21}$$

where Q is shown in Eq (12), and $\xi\left(t\right)$ is applied as the following definitions and conditions:

$$\xi\left(t\right)=\left[\eta_{\mathrm{m1}}\quad \eta_{\mathrm{m2}}\quad \eta_{\mathrm{m3}}\quad \left|\eta_{\mathrm{m1}}\right|^{\frac{3}{2}}\mathrm{sgn}\left(\eta_{\mathrm{m1}}\right)\quad \left|\eta_{\mathrm{m1}}\right|^{\frac{5}{4}}\mathrm{sgn}\left(\eta_{\mathrm{m1}}\right)\quad \left|\eta_{\mathrm{m1}}\right|^{\frac{3}{4}}\mathrm{sgn}\left(\eta_{\mathrm{m1}}\right)\quad \left|\eta_{\mathrm{m1}}\right|^{\frac{1}{2}}\mathrm{sgn}\left(\eta_{\mathrm{m1}}\right)\right]$$

Based on the Lyapunov stability principle, the solutions of the inequality $Q\le 0$ represent the appropriate positive definite constants k_1–k_9 and parameters β_{m1}, β_{m2}, and β_{m3}. Therefore, the estimation stability of error system (10) is assured because the estimation error converges to the neighborhood of the origin.

3.2. Design of the BLF-based controller

In this section, the estimations of interference factors obtained by the nonlinear ESO are used for compensation in the BLF-based controller in conjunction with the constraints on the state variables. Here, the controllers are designed separately for the master and slave manipulators because these are heterogeneous systems.

For the master manipulator system (1) with the applied correspondences (3), the position and speed $X_{\mathrm{m}j}$, j = 1, 2 of the manipulator system are assumed to be bounded in actual applications, and satisfy $\left|X_{\mathrm{m}j}\right|<k_{\mathrm{m}j}$, where $k_{\mathrm{m}j}$ is a positive definite constant. The errors associated with X_{m1} and X_{m2} are assumed to be respectively definable as $\chi_{\mathrm{m1}}=X_{\mathrm{m1}}-X_{\mathrm{md}}$ and $\chi_{\mathrm{m2}}=X_{\mathrm{m2}}-\alpha_{\mathrm{m1}}$, where

$X_{\mathrm{md}} = q_{\mathrm{s}}\left(t - T_{\mathrm{s}}\right)$ is the tracking trajectory of the master manipulator, that is, the reference signal, T_{s} is the transmission delay of the signal from the end to the master, and α_{m1} is the virtual controller. In this study, the virtual controller is an intermediate design variable used to simplify the control problem of complex systems by decomposing high-order systems into lower-order subsystems for step-by-step design and analysis. These assumptions are specified and validated as follows.

Assumption 2: Assume that appropriate positive definite constants $k_{\mathrm{m}j}$ exist that ensure that $\left|\chi_{\mathrm{m}j}\right| < k_{\mathrm{m}j}$ is satisfied.

Assumption 3: Assume that appropriate positive definite constants A_{m0} and A_{m1} exist that can guarantee that the conditions $\left|X_{\mathrm{md}}\right| \le A_{\mathrm{m0}} < k_{m1}$ and $\left|\dot{X}_{\mathrm{md}}\right| \le A_{\mathrm{m1}}$ are satisfied.

Step 1: Select the following positive definite candidate BLF:

$$V_{\mathrm{m1}} = \frac{1}{2}\log\left(\frac{k_{\mathrm{m1}}^2}{k_{\mathrm{m1}}^2 - \chi_{\mathrm{m1}}^2}\right) \tag{22}$$

Taking the derivative of V_{m1} with respect to time yields the following:

$$\begin{aligned}\dot{V}_{\mathrm{m1}} &= \frac{\chi_{\mathrm{m1}}\dot{\chi}_{\mathrm{m1}}}{k_{\mathrm{m1}}^2 - \chi_{\mathrm{m1}}^2} \\ &= k_{\chi_{\mathrm{m1}}}\left(\chi_{\mathrm{m2}} + \alpha_{\mathrm{m1}} - \dot{X}_{\mathrm{md}}\right)\end{aligned} \tag{23}$$

Here, $k_{\chi_{\mathrm{m1}}} = \frac{\chi_{\mathrm{m1}}}{k_{\mathrm{m1}}^2 - \chi_{\mathrm{m1}}^2}$. The virtual controller α_{m1} is designed as follows:

$$\alpha_{\mathrm{m1}} = -K_{\mathrm{m1}}\chi_{\mathrm{m1}} + \dot{X}_{\mathrm{md}} \tag{24}$$

Substituting (24) in (23) yields the following:

$$\dot{V}_{\mathrm{m1}} = -k_{\chi_{\mathrm{m1}}}K_{\mathrm{m1}}\chi_{\mathrm{m1}} + k_{\chi_{\mathrm{m1}}}\chi_{\mathrm{m2}} \tag{25}$$

Step 2: Select the following positive definite candidate BLF:

$$V_{\mathrm{m}} = V_{\mathrm{m1}} + \frac{1}{2}\log\left(\frac{k_{\mathrm{m2}}^2}{k_{\mathrm{m2}}^2 - \chi_{\mathrm{m2}}^2}\right) \tag{26}$$

According to (3) and (25), taking the derivative of V_{m} with respect to time yields the following.

$$\begin{aligned}\dot{V}_{\mathrm{m}} &= \dot{V}_{\mathrm{m1}} + \frac{\chi_{\mathrm{m2}}\dot{\chi}_{\mathrm{m2}}}{k_{\mathrm{m2}}^2 - \chi_{\mathrm{m2}}^2} \\ &= -k_{\chi_{\mathrm{m1}}} K_{\mathrm{m1}} \chi_{\mathrm{m1}} + k_{\chi_{\mathrm{m1}}} \chi_{\mathrm{m2}} + k_{\chi_{\mathrm{m2}}} \left(\dot{X}_{\mathrm{m2}} - \dot{\alpha}_{\mathrm{m1}} \right) \\ &= -k_{\chi_{\mathrm{m1}}} K_{\mathrm{m1}} \chi_{\mathrm{m1}} + k_{\chi_{\mathrm{m1}}} k_{\chi_{\mathrm{m2}}} \left(k_{\mathrm{m2}}^2 - \chi_{\mathrm{m2}}^2 \right) + k_{\chi_{\mathrm{m2}}} \left(M_{\mathrm{m}}^{-1} \tau_{\mathrm{m}} + F_{\mathrm{m}} - \dot{\alpha}_{\mathrm{m1}} \right)\end{aligned} \tag{27}$$

Here, $k_{\chi_{\mathrm{m2}}} = \frac{\chi_{\mathrm{m2}}}{k_{\mathrm{m2}}^2 - \chi_{\mathrm{m2}}^2}$. The derivative of α_{m1} with respect to time is approximated by the tracking differentiator. The tracking differentiator is an algorithm for estimating signal derivatives based on PID control and improved by Han [18], which can accurately track and output the differential value of signals in the presence of noise. The details are as follows:

$$\begin{aligned}\dot{v}_{\mathrm{m1}} &= v_{\mathrm{m2}} \\ \dot{v}_{\mathrm{m2}} &= -r \left| v_{\mathrm{m1}} - v_{\mathrm{m0}} \right|^{\frac{1}{2}} sign\left(v_{\mathrm{m1}} - v_{\mathrm{m0}} \right) - v_{\mathrm{m2}}\end{aligned} \tag{28}$$

Setting $v_{\mathrm{m0}} = \alpha_{\mathrm{m1}}$ indicates that v_{m1} and v_{m2} are the estimated values of α_{m1} and its derivative $\dot{\alpha}_{\mathrm{m1}}$, respectively (i.e., $\hat{\alpha}_{\mathrm{m1}} = v_{\mathrm{m1}}$ and $\hat{\dot{\alpha}}_{\mathrm{m1}} = v_{\mathrm{m2}}$). Therefore, the estimation error $\tilde{\dot{\alpha}}_{\mathrm{m1}} = \dot{\alpha}_{\mathrm{m1}} - \hat{\dot{\alpha}}_{\mathrm{m1}}$ is assumed to be bounded, and satisfies the condition $\left| \tilde{\dot{\alpha}}_{\mathrm{m1}} \right| \le \mu_{\mathrm{m1}}$, where μ_{m1} is an appropriate positive definite constant. Finally, the input controller τ_{m} of the master manipulator is designed as:

$$\tau_{\mathrm{m}} = M_{\mathrm{m}} \left[-K_{\mathrm{m2}} \chi_{\mathrm{m2}} - k_{\chi_{\mathrm{m2}}} \left(k_{\mathrm{m2}}^2 - \chi_{\mathrm{m2}}^2 \right) - \hat{F}_{\mathrm{m}} + \hat{\dot{\alpha}}_{\mathrm{m1}} \right] \tag{29}$$

where $\hat{F}_{\mathrm{m}}$ is the value of F_{m} estimated by the nonlinear ESO presented in the previous section. Therefore, (27) can be expressed as follows.

$$\dot{V}_{\mathrm{m}} = -k_{\chi_{\mathrm{m1}}} K_{\mathrm{m1}} \chi_{\mathrm{m1}} - k_{\chi_{\mathrm{m2}}} K_{\mathrm{m2}} \chi_{\mathrm{m2}} + k_{\chi_{\mathrm{m2}}} \tilde{F}_{\mathrm{m}} + k_{\chi_{\mathrm{m2}}} \tilde{\dot{\alpha}}_{\mathrm{m1}} \tag{30}$$

where $\tilde{F}_{\mathrm{m}}$ is the estimation error of F_{m} estimated by the nonlinear ESO presented in the previous section. For the slave manipulator system (2) with the applied correspondences (4), the position, angular position, speed, and angular speed $X_{\mathrm{s}j}$, j = 1, 2, 3, 4 of the system are assumed to be bounded in practical applications, and satisfy the condition $\left| X_{sj} \right| < k_{\mathrm{s}j}$, where k_{sj} is a positive definite constant. The errors in X_{s1}, X_{s2}, X_{s3}, and X_{s4} are assumed to be respectively definable as $\chi_{\mathrm{s1}} = X_{\mathrm{s1}} - X_{\mathrm{sd}}$, $\chi_{\mathrm{s2}} = X_{\mathrm{s2}} - \alpha_{\mathrm{s1}}$, $\chi_{\mathrm{s3}} = X_{\mathrm{s3}} - \alpha_{\mathrm{s2}}$, and $\chi_{\mathrm{s4}} = X_{\mathrm{s4}} - \alpha_{\mathrm{s3}}$, where the reference signal $X_{\mathrm{sd}} = q_{\mathrm{m}}\left(t - T_{\mathrm{m}} \right)$ is

the tracking trajectory of the slave manipulator that accounts for the transmission delay T_{m} of the signal from the master manipulator to the slave manipulator, and the control signal α_{sj}, $j=1,2,3$ of the virtual controller. These assumptions are specified and validated as follows.

Assumption 4: Assume that appropriate positive definite constants k_{sj} exist that ensure that $\left|X_{sj}\right|<k_{sj}$ is satisfied.

Assumption 5: Assume that appropriate positive definite constants A_{s0} and A_{s1} exist that ensure that the conditions $\left|X_{sd}\right|\le A_{s0}<\bar{k}_{s1}$ and $\left|\dot{X}_{sd}\right|\le A_{s1}$ are satisfied.

Step 1: Select the following positive definite candidate BLF**:**

$$V_{s1}=\frac{1}{2}\log\left(\frac{k_{s1}^2}{k_{s1}^2-\chi_{s1}^2}\right) \tag{31}$$

The derivative of V_{s1} with respect to time can be obtained as follows:

$$\begin{aligned}\dot{V}_{s1}&=\frac{\chi_{s1}\dot{\chi}_{s1}}{k_{s1}^2-\chi_{s1}^2}\\&=k_{\chi_{s1}}\left(\chi_{s2}+\alpha_{s1}-\dot{X}_{sd}\right)\end{aligned} \tag{32}$$

Here, $k_{\chi_{s1}}=\frac{\chi_{s1}}{k_{s1}^2-\chi_{s1}^2}$, while the other terms $k_{\chi_{sj}}=\frac{\chi_{sj}}{k_{sj}^2-\chi_{sj}^2}$, $j=2,3,4$, will be used below. The virtual controller α_{s1} is designed as follows.

$$\alpha_{s1}=-K_{s1}\chi_{s1}+\dot{X}_{sd} \tag{33}$$

Substituting (33) in (32) yields the following:

$$\dot{V}_{s1}=-k_{\chi_{s1}}K_{s1}\chi_{s1}+k_{\chi_{s1}}\chi_{s2} \tag{34}$$

Step 2: Select the following positive definite candidate BLF:

$$V_{s2}=V_{s1}+\frac{1}{2}\log\left(\frac{k_{s2}^2}{k_{s2}^2-\chi_{s2}^2}\right) \tag{35}$$

According to Eqs (4) and (34), taking the derivative of V_{s2} with respect to time yields the following:

$$\begin{aligned}\dot{V}_{s2} &= \dot{V}_{s1} + \frac{\chi_{s2}\dot{\chi}_{s2}}{k_{s2}^2 - \chi_{s2}^2} \\ &= -k_{\chi_{s1}} K_{s1}\chi_{s1} + k_{\chi_{s1}}\chi_{s2} + k_{\chi_{s2}}\left(\dot{X}_{s2} - \dot{\alpha}_{s1}\right) \\ &= -k_{\chi_{s1}} K_{s1}\chi_{s1} + k_{\chi_{s1}} k_{\chi_{s2}}\left(k_{s2}^2 - \chi_{s2}^2\right) + k_{\chi_{s2}}\left(M_s^{-1}K_s\left(\chi_{s3} + \alpha_{s2} - X_{s1}\right) + F_s - \dot{\alpha}_{s1}\right)\end{aligned} \tag{36}$$

Again, the estimated values of α_{s1} and $\dot{\alpha}_{s1}$ are respectively obtained from v_{s1} and v_{s2} (i.e., $\hat{\alpha}_{s1} = v_{s1}$ and $\hat{\dot{\alpha}}_{s1} = v_{s2}$) using the tracking differentiator (28) with $v_{s0} = \alpha_{s1}$. Therefore, the estimation error $\tilde{\dot{\alpha}}_{s1} = \dot{\alpha}_{s1} - \hat{\dot{\alpha}}_{s1}$ is assumed to be bounded and satisfies $\left|\tilde{\dot{\alpha}}_{s1}\right| \le \mu_{s1}$, where μ_{s1} is an appropriate positive definite constant. Then, the virtual controller α_{s2} of the slave manipulator is designed as:

$$\alpha_{s2} = \frac{1}{K_s} M_s\left[-K_{s2}\chi_{s2} + \hat{\dot{\alpha}}_{s1} - k_{\chi_{s2}}\left(k_{s2}^2 - \chi_{s2}^2\right) - \hat{F}_s\right] + X_{s1} \tag{37}$$

where $\hat{F}_s$ is the value of F_s estimated by the nonlinear ESO. Therefore, substituting (37) in (36) yields.

$$\dot{V}_{s2} = -k_{\chi_{s1}} K_{s1}\chi_{s1} - k_{\chi_{s2}} K_{s2}\chi_{s2} + M_s^{-1}K_s k_{\chi_{s2}}\chi_{s3} + k_{\chi_{s2}}\tilde{F}_s + k_{\chi_{s2}}\tilde{\dot{\alpha}}_{s1} \tag{38}$$

where $\tilde{F}_s$ is the estimation error of F_s estimated by the nonlinear ESO presented in the previous section.

Step 3: Select the following positive definite candidate BLF:

$$V_{s3} = V_{s2} + \frac{1}{2}\log\left(\frac{k_{s3}^2}{k_{s3}^2 - \chi_{s3}^2}\right) \tag{39}$$

According to Eqs (4) and (38), the derivative of V_{s3} with respect to time can be obtained as follows:

$$\begin{aligned}\dot{V}_{s3} &= \dot{V}_{s2} + \frac{\chi_{s3}\dot{\chi}_{s3}}{k_{s3}^2 - \chi_{s3}^2} \\ &= -k_{\chi_{s1}} K_{s1}\chi_{s1} - k_{\chi_{s2}} K_{s2}\chi_{s2} + M_s^{-1}K_s k_{\chi_{s2}}\chi_{s3} + k_{\chi_{s2}}\tilde{F}_s + k_{\chi_{s2}}\tilde{\dot{\alpha}}_{s1} \\ &\quad + k_{\chi_{s3}}\left(\chi_{s4} + \alpha_{s3} - \dot{\alpha}_{s2}\right)\end{aligned} \tag{40}$$

The values of $\hat{\alpha}_{s2} = v_{s1}$ and $\hat{\dot{\alpha}}_{s2} = v_{s2}$ are obtained using the tracking differentiator (28) with $v_{s0} = \alpha_{s2}$. Therefore, the estimation error $\tilde{\dot{\alpha}}_{s2} = \dot{\alpha}_{s2} - \hat{\dot{\alpha}}_{s2}$ is assumed to be bounded and satisfies $\left|\tilde{\dot{\alpha}}_{s2}\right| \le \mu_{s2}$, where μ_{s2} is an appropriate positive definite constant. Then, the virtual controller α_{s3} of

the slave manipulator is designed as follows:

$$\alpha_{s3} = -K_{s3}\chi_{s3} + \hat{\dot{\alpha}}_{s2} - M_s^{-1}K_s k_{\chi_{s2}}\left(k_{s3}^2 - \chi_{s3}^2\right) \tag{41}$$

Therefore, (40) can be expressed as follows:

$$\begin{aligned}\dot{V}_{s3} = &-k_{\chi_{s1}}K_{s1}\chi_{s1} - k_{\chi_{s2}}K_{s2}\chi_{s2} - k_{\chi_{s3}}K_{s3}\chi_{s3} + k_{\chi_{s3}}\chi_{s4}\\ &+ k_{\chi_{s2}}\tilde{F}_s + k_{\chi_{s2}}\tilde{\dot{\alpha}}_{s1} + k_{\chi_{s3}}\tilde{\dot{\alpha}}_{s2}\end{aligned} \tag{42}$$

Step 4: Select the following positive definite candidate BLF:

$$V_s = V_{s3} + \frac{1}{2}\log\left(\frac{k_{s4}^2}{k_{s4}^2 - \chi_{s4}^2}\right) \tag{43}$$

According to Eqs (4) and (42), the derivative of V_s with respect to time can be obtained as follows:

$$\begin{aligned}\dot{V}_s &= \dot{V}_{s3} + \frac{\chi_{s4}\dot{\chi}_{s4}}{k_{s4}^2 - \chi_{s4}^2}\\ &= -k_{\chi_{s1}}K_{s1}\chi_{s1} - k_{\chi_{s2}}K_{s2}\chi_{s2} - k_{\chi_{s3}}K_{s3}\chi_{s3} + k_{\chi_{s3}}k_{\chi_{s4}}\left(k_{s4}^2 - \chi_{s4}^2\right)\\ &\quad + k_{\chi_{s2}}\tilde{F}_s + k_{\chi_{s2}}\tilde{\dot{\alpha}}_{s1} + k_{\chi_{s3}}\tilde{\dot{\alpha}}_{s2} + k_{\chi_{s4}}\left(J_s^{-1}\tau_s + F_f - \dot{\alpha}_{s3}\right)\end{aligned} \tag{44}$$

The values of $\hat{\alpha}_{s3} = v_{s1}$ and $\hat{\dot{\alpha}}_{s3} = v_{s2}$ are obtained using the tracking differentiator (28) with $v_{s0} = \alpha_{s3}$. Therefore, the estimation error $\tilde{\dot{\alpha}}_{s3} = \dot{\alpha}_{s3} - \hat{\dot{\alpha}}_{s3}$ is assumed to be bounded and satisfies $\left|\tilde{\dot{\alpha}}_{s3}\right| \le \mu_{s3}$, where μ_{s3} is an appropriate positive definite constant. Then, the input controller τ_s of the slave manipulator is designed as:

$$\tau_s = J_s\left(-K_{s4}\chi_{s4} + \hat{\dot{\alpha}}_{s3} - k_{\chi_{s3}}\left(k_{s4}^2 - \chi_{s4}^2\right) - \hat{F}_f\right) \tag{45}$$

where $\hat{F}_f$ is the value of F_f estimated by the nonlinear ESO. Therefore, (44) can be expressed as:

$$\begin{aligned}\dot{V}_s = &-k_{\chi_{s1}}K_{s1}\chi_{s1} - k_{\chi_{s2}}K_{s2}\chi_{s2} - k_{\chi_{v3}}K_{s3}\chi_{s3} - k_{\chi_{s4}}K_{s4}\chi_{s4}\\ &+ k_{\chi_{s2}}\tilde{F}_s + k_{\chi_{s2}}\tilde{\dot{\alpha}}_{s1} + k_{\chi_{s3}}\tilde{\dot{\alpha}}_{s2} + k_{\chi_{s4}}\tilde{\dot{\alpha}}_{s3} + k_{\chi_{s4}}\tilde{F}_f\end{aligned} \tag{46}$$

where $\tilde{F}_f$ is the estimation error of F_f estimated by the nonlinear ESO presented in the previous section. The control block diagram of the teleoperation system with controllers (29) and (45) is presented in Figure 1. Figure 1 delineates the advanced teleoperation control framework between a Master and

Slave robot. Here, both robots employ ESOs to estimate uncertainties and a BLF-based controller for precision. The network delay in command transmission is explicitly represented, showcasing the integrated approach in handling flexible joint uncertainties. Both robots operate within full state constraints, highlighting the strategy's emphasis on synchronized and reliable robotic interactions.

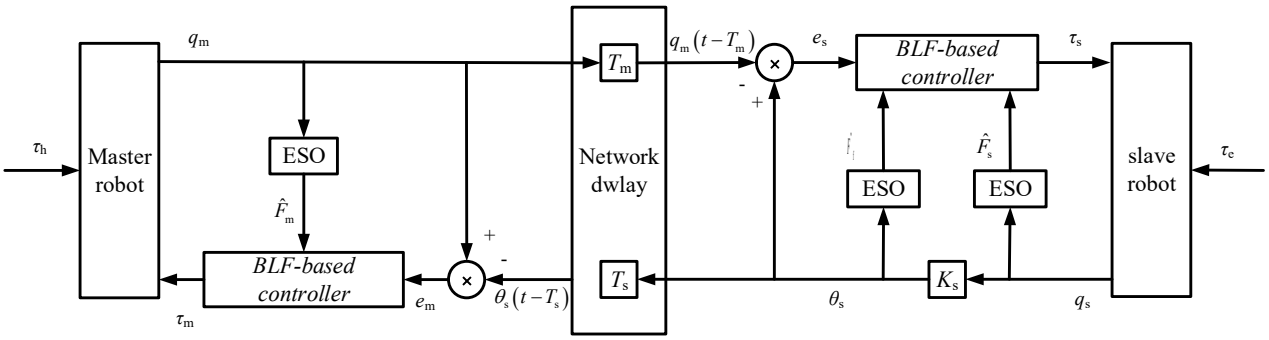

Figure 1. Control block diagram of the teleoperation system with input controllers τ_m and τ_s.

Theorem 2: *Assume that the teleoperation system satisfies Assumptions 2–5. Then,* under *the virtual controller* α_{ij}*, where j = 1, 2 when i = m, and j = 1, 2, 3, 4 when i = s, and the input controllers* τ_m *and* τ_s*, all variables of the closed-loop system are bounded and do not exceed their constraints if two positive definite constants* a *and* b *exist that satisfy the following conditions.*

$$\begin{aligned} a &= \min\left(K_{m1}, K_{m2}, K_{s1}, K_{s2}, K_{s3}, K_{s4}\right) \\ b &= \min\left(\mu_{m1}, \mu_{s1}, \mu_{s2}, \mu_{s3}\right)\left(k_{\chi_{m1}} + k_{\chi_{s2}} + k_{\chi_{s3}} + k_{\chi_{s4}}\right) + k_{\chi_{m2}}\tilde{F}_m + k_{\chi_{s2}}\tilde{F}_s + k_{\chi_{s4}}\tilde{F}_f \end{aligned} \tag{47}$$

Proof: Choose the following Lyapunov function:

$$V = V_m + V_s \tag{48}$$

When $\left|\chi_{ij}\right| < k_{ij}$, positive definite constants must exist that satisfy the condition $\frac{k_{ij}^2}{k_{ij}^2 - \chi_{ij}^2} > \frac{\chi_{ij}^2}{k_{ij}^2 - \chi_{ij}^2}$. Therefore, according to Eqs (30) and (46), the derivative of V with respect to time can be obtained as follows:

$$\dot{V} \le -aV + b \tag{49}$$

Multiplying both sides of inequality (49) by e^{at} yields the following form:

$$d\left(V\right)e^{at}\left/dt\le be^{at}\right. \tag{50}$$

Furthermore, integrating (50) over the interval $\left[0,t\right]$ yields the following:

$$V\left(t\right)\le\left(V\left(0\right)-\frac{b}{a}\right)e^{-at}+\frac{b}{a}\le V\left(0\right)+\frac{b}{a} \tag{51}$$

Given that $\hat{F}_{\mathrm{m}}$, $\hat{F}_{\mathrm{s}}$, $\hat{F}_{\mathrm{f}}$ and $\hat{\alpha}_{ij}$ are bounded, $\left|X_{i1}\right|<k_{i1}+A_{i0}<\overline{k}_{i1}$ can be obtained from $\chi_{i1}=X_{i1}-X_{i\mathrm{d}}$ and $X_{i\mathrm{d}}\le A_{i0}$. The boundedness of χ_{i1} and $\dot{X}_{i\mathrm{d}}$ ensures that α_{i1} is bounded and $\alpha_{i1}\le\overline{\alpha}_{i1}$. Similarly, $\left|X_{i2}\right|<k_{i2}+\overline{\alpha}_{i1}<k_{i2}$ can be obtained from $\chi_{i2}=X_{i2}-\alpha_{i1}$, and $\left|X_{\mathrm{s}3}\right|<k_{\mathrm{s}3}$, and $\left|X_{\mathrm{s}4}\right|<k_{\mathrm{s}4}$ can be obtained in the same way. Furthermore, the input controller signals τ_{m} and τ_{s} are bounded according to their definitions in Eqs (29) and (45), respectively, where τ_{m} is a function of $\chi_{\mathrm{m}2}$, $\hat{F}_{\mathrm{m}}$, and $\hat{\dot{\alpha}}_{\mathrm{m}1}$, and τ_{s} is a function of $\chi_{\mathrm{s}4}$, $\hat{F}_{\mathrm{f}}$, and $\hat{\dot{\alpha}}_{\mathrm{s}3}$. Therefore, all signals of the system, namely τ_{m}, τ_{s}, and X_{ij}, are bounded and meet their constraints.

4. Experimental platform and analysis of experimental results

The experimental teleoperation platform employed for testing the effectiveness of the proposed control strategy is presented in Figure 2, and consisted of two Phantom Premium 1.5HF (SensAble Technologies, Inc.) three-degrees-of-freedom robotic arms. The Phantom Premium 1.5HF arm has three rotating joints, each consisting of three parts of a gear motor encoder, which can feel or follow the movement of the controlled object on three perpendicular axes in space. The controllers and all software were implemented in MATLAB, and the flexible joint from the slave manipulator was realized by a virtual module in MATLAB.

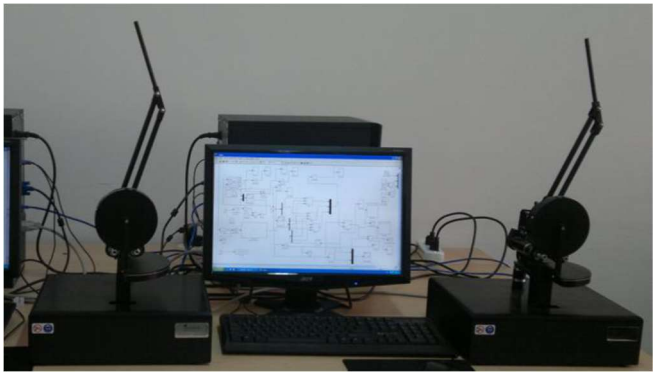

Figure 2. Experimental platform employed for testing the teleoperation system.

Angle sensors were installed at each joint on the master and slave end of the three-degree-of-freedom manipulator to measure the required angle. For the process of experimental verification, the delays were set to $T_m = T_s = 200$ ms. The appropriate parameters were obtained through experiments and set as:

$$\varepsilon = 1.05,\quad \beta_{m1} = \beta_{s1} = \begin{bmatrix} 210 & 0 & 0 \\ 0 & 250 & 0 \\ 0 & 0 & 200 \end{bmatrix},\quad \beta_{m2} = \beta_{s2} = \begin{bmatrix} 2.5 & 0 & 0 \\ 0 & 1.5 & 0 \\ 0 & 0 & 2.5 \end{bmatrix},\quad \beta_{m3} = \beta_{s3} = \begin{bmatrix} 0.0015 & 0 & 0 \\ 0 & 0.0025 & 0 \\ 0 & 0 & 0.0025 \end{bmatrix}.$$

The parameters of the master controller are selected as: $K_{m1} = \begin{bmatrix} 5 & 0 & 0 \\ 0 & 7.8 & 0 \\ 0 & 0 & 6.8 \end{bmatrix}$, $K_{m2} = \begin{bmatrix} 0.71 & 0 & 0 \\ 0 & 0.3 & 0 \\ 0 & 0 & 0.3 \end{bmatrix}$, $k_{m1} = \begin{bmatrix} 1.4 \\ 1.4 \\ 1.3 \end{bmatrix}$, $k_{m2} = \begin{bmatrix} 1.5 \\ 2.8 \\ 1.5 \end{bmatrix}$. The stiffness coefficient for the flexible joint of the slave manipulator was set as $K_s = \begin{bmatrix} 12 & 0 & 0 \\ 0 & 12 & 0 \\ 0 & 0 & 12 \end{bmatrix}$, while the slave controller parameters were set as $K_{s1} = \begin{bmatrix} 1.1 & 0 & 0 \\ 0 & 0.9 & 0 \\ 0 & 0 & 0.9 \end{bmatrix}$, $K_{s2} = \begin{bmatrix} 0.7 & 0 & 0 \\ 0 & 0.5 & 0 \\ 0 & 0 & 0.7 \end{bmatrix}$, $K_{s3} = \begin{bmatrix} 3.1 & 0 & 0 \\ 0 & 0.9 & 0 \\ 0 & 0 & 0.9 \end{bmatrix}$, $K_{s4} = \begin{bmatrix} 14.5 & 0 & 0 \\ 0 & 19.5 & 0 \\ 0 & 0 & 19.5 \end{bmatrix}$, $k_{s1} = \begin{bmatrix} 0.4 \\ 0.5 \\ 0.5 \end{bmatrix}$, $k_{s2} = \begin{bmatrix} 0.5 \\ 0.5 \\ 0.5 \end{bmatrix}$, $k_{s3} = \begin{bmatrix} 0.4 \\ 0.4 \\ 0.4 \end{bmatrix}$, $k_{s4} = \begin{bmatrix} 0.5 \\ 0.3 \\ 0.3 \end{bmatrix}$.

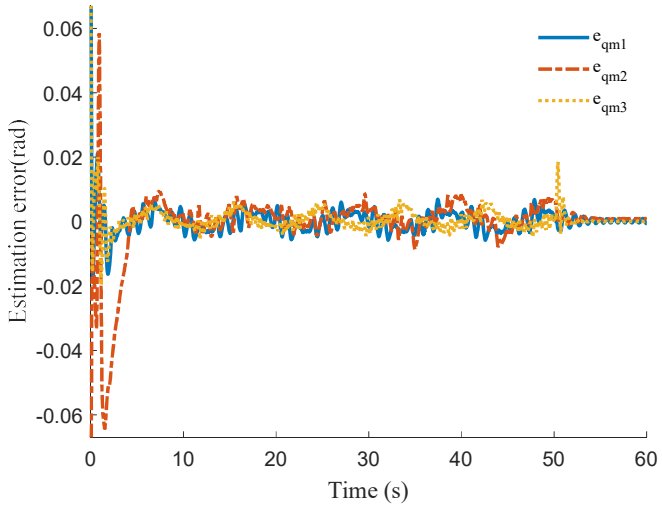

Figure 3. Position estimation error of the master manipulator.

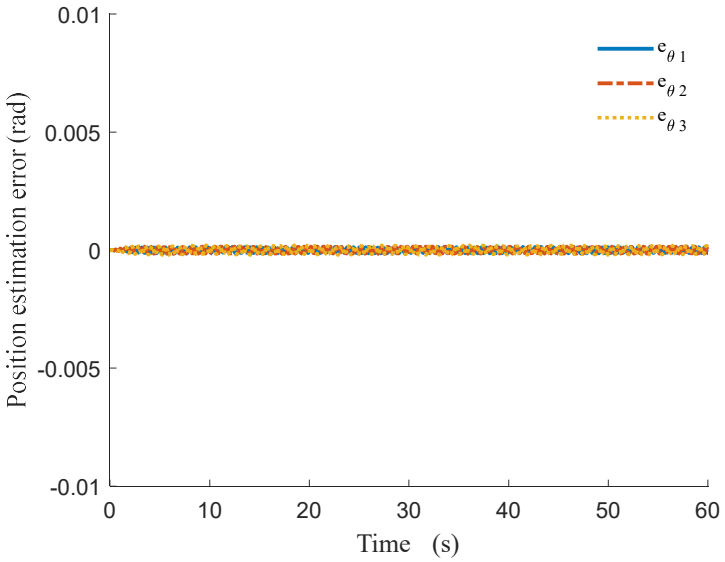

Figure 4. Position estimation error of the slave manipulator at the motor.

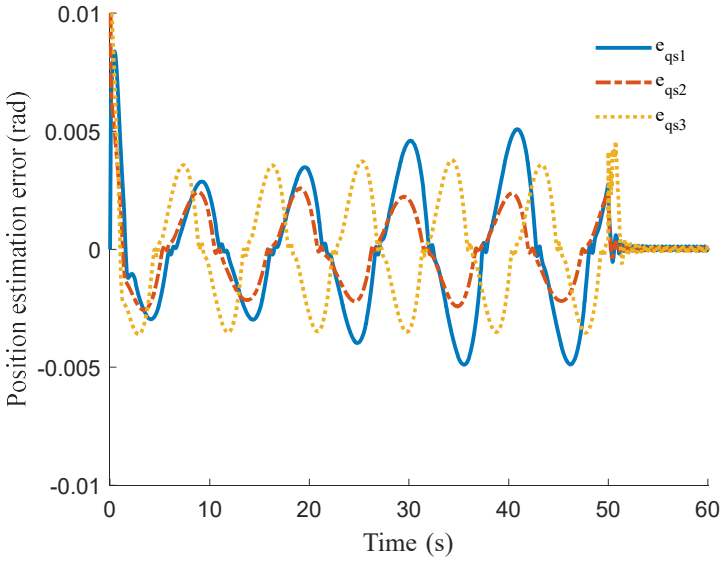

Figure 5. Position estimation error of the slave manipulator at the chain rod.

In the experimental evaluation, Figures 3–5 delve into the position estimation errors of both the master and slave manipulators over three degrees of freedom. Specifically, Figure 3 showcases the master manipulator's position errors, which consistently remain below ± 0.02 rad. Figures 4 and 5, representing the slave manipulator's errors at its motors and chain rod respectively, confirm errors below ± 0.05 rad. These figures underline the nonlinear ESO's superior capability in accurately estimating the positions of both manipulators.

Figure 6, illustrating the control inputs, highlights a synchronized control approach between the master and slave manipulators. Their control signals exhibit sine wave-like consistencies, reinforcing the effectiveness of the implemented synchronization.

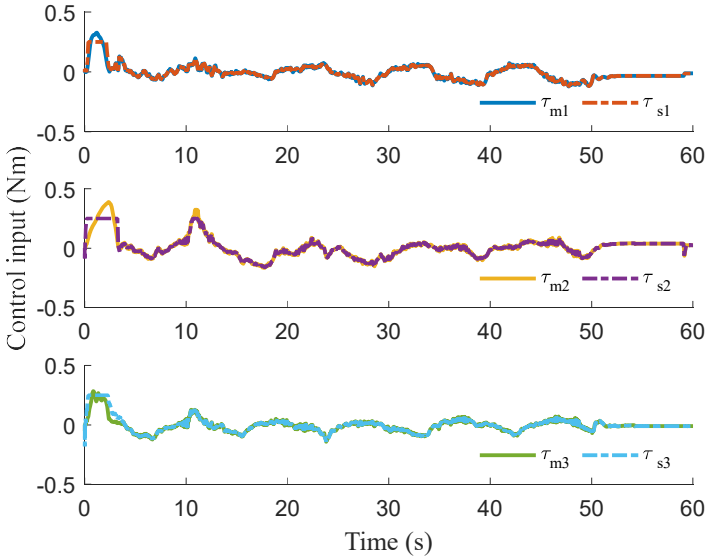

Figure 6. Control input from the master and the slave manipulator. (In the figure, the solid line represents the master manipulator and the dotted line represents the slave manipulator.)

The master and slave manipulator positions over time are depicted in Figure 7. Notably, their positions mirror each other closely, with a mere average deviation of ± 0.02 rad as substantiated in Figure 8. Upon halting the manipulator motion after 50 seconds, the tracking error rapidly zeroes out, underscoring the controller's adeptness in position synchronization.

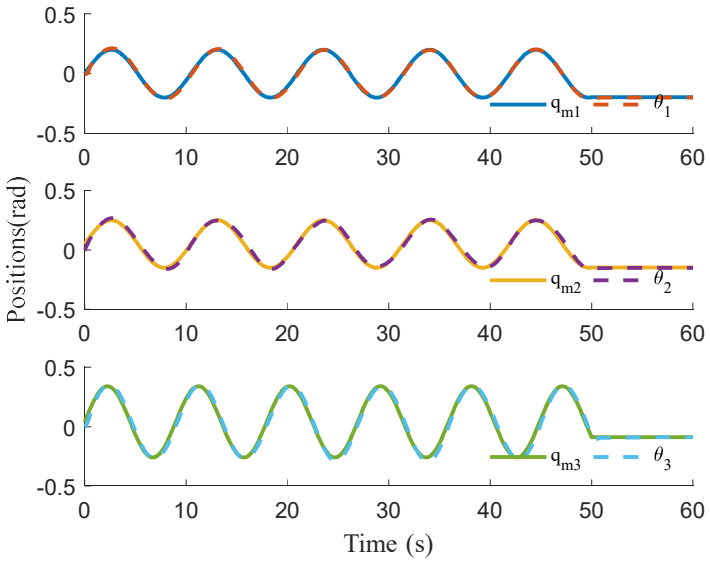

Figure 7. Positions of the master and slave manipulators over time. (In the figure, the solid line represents the master manipulator and the dotted line represents the slave manipulator.)

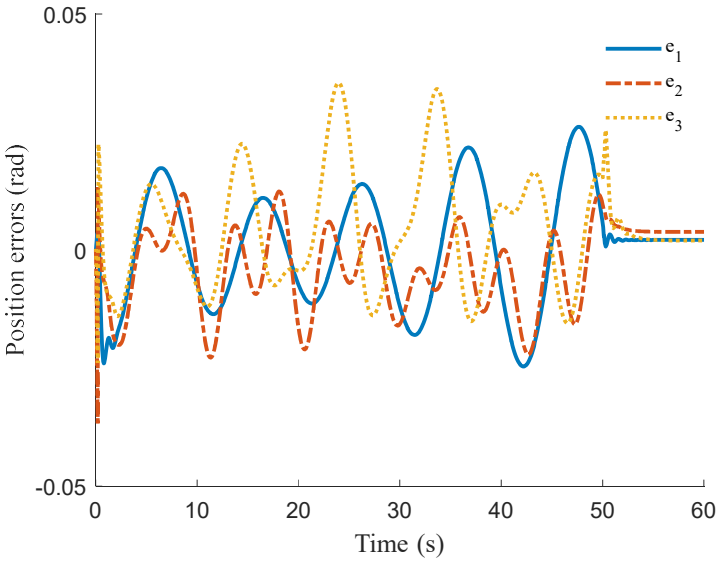

Figure 8. Tracking errors between the positions of the master and slave manipulators.

Figures 9 and 10 further emphasize the system's stability. Despite initially larger tracking errors, they swiftly reduce to a maximum of ± 0.05 rad and approach zero when the motion is halted after 50 seconds, indicating minimal influence from external forces.

To summarize, these experimental findings bolster the merits of the proposed control strategy. It not only achieves precise position estimations and effective synchronization, but also remains resilient against potential disturbances. This culmination holds significant promise for enhancing teleoperation systems in intricate operational landscapes.

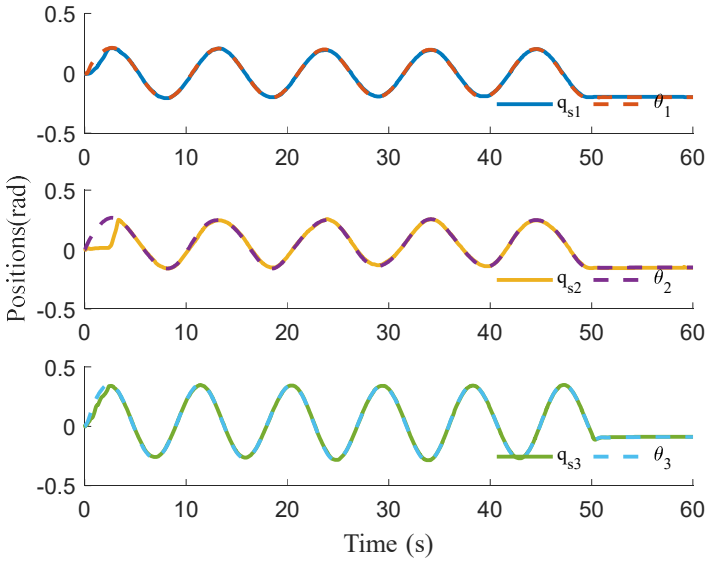

Figure 9. Motor and chain rod positions of the slave manipulator over time. (The solid and dotted lines in the figure represent motor and chain rod positions of the slave manipulator, respectively.)

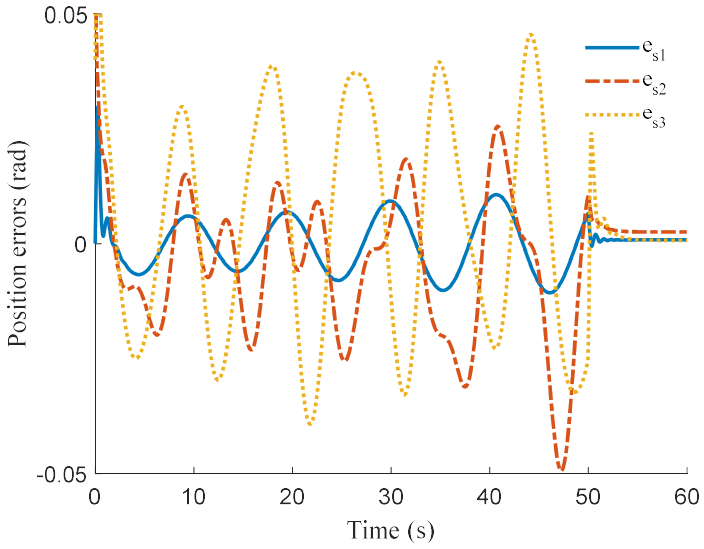

Figure 10. Tracking errors between the positions of the motor and chain rod of the slave manipulator.

5. Conclusions

This research marks a significant stride in the realm of teleoperation systems specifically designed for robotic manipulators with flexible joints. Our primary focus revolves around investigating the feasibility of a pose control strategy for teleoperated systems with flexible joints. This strategy is anchored on the integration of a nonlinear Extended State Observer (ESO) with a Barrier Lyapunov Function (BLF).

The efficacy of this novel approach is convincingly demonstrated by our experimental findings. Specifically, in a master-slave operating system, the slave exhibits exceptional synchronization capabilities with high precision. The position estimation errors in the master-slave operation consistently remain within ± 0.05 radians, particularly at the chain rod where it is even less than ± 0.01 radians. Even in complex scenarios involving flexible joints, this level of precision showcases the robustness and potential of our integration strategy.

It is essential to highlight that the crux of this study was to explore the feasibility of the aforementioned control strategy. Therefore, instead of comparing it with existing methodologies, we have dedicated our efforts to comprehensively understand and elucidate its intrinsic merits.

As we pave the path forward, we envision delving deeper into enhancing the nuances of our approach. While we have not directly compared our method with industry benchmarks in this study, future endeavors might involve such comparative analyses. Nonetheless, our primary goal remains: to further elucidate, validate, and promote the unique potential and adaptability of our teleoperation strategy across diverse operational scenarios.

Use of AI tools declaration

The authors declare they have not used Artificial Intelligence (AI) tools in the creation of this article.

Acknowledgements

This paper is supported by National Natural Science Foundation of China under grant No. 52305066.

Conflict of interest

The authors declare there is no conflict of interest.

References

1. G. Li, F. Caponetto, E. Del Bianco, V. Katsageorgiou, I. Sarakoglou, N. G. Tsagarakis, A workspace limit approach for teleoperation based on signed distance function, *IEEE Rob. Autom. Lett.*, **6** (2021), 5589–5596. https://doi.org/10.1109/LRA.2021.3079810
2. M. S. Mahmoud, M. Maaruf, Prescribed performance output feedback synchronisation control of bilateral teleoperation system with actuator nonlinearities, *Int. J. Syst. Sci.*, **52** (2021), 3115–3127. https://doi.org/10.1080/00207721.2021.1921308
3. Z. Deng, S. Zhang, Y. Guo, H. Jiang, X. Zheng, B. He, Assisted teleoperation control of robotic endoscope with visual feedback for nasotracheal intubation, *Rob. Auton. Syst.*, **172** (2024), 104586. https://doi.org/10.1016/j.robot.2023.104586
4. M. Azeez, A. A. Abdelhaleem, S. Elnaggar, K. A. F. Moustafa, K. R. Atia, Optimized sliding mode controller for trajectory tracking of flexible joints three-link manipulator with noise in input and output, *Sci. Rep.*, **13** (2023), 12518. https://doi.org/10.1038/s41598-023-38855-7
5. M. Shi, J. Yu, T. Zhang, Command filter-based adaptive control of flexible-joint manipulator with input saturation and output constraints, *Asian J. Control*, **2023** (2023), forthcoming. https://doi.org/10.1002/asjc.3177
6. J. Reinecke, A. Dietrich, A. Shu, B. Deutschmann, M. Hutter, A robotic torso joint with adjustable linear spring mechanism for natural dynamic motions in a differential-elastic arrangement, *IEEE Rob. Autom. Lett.*, **7** (2022), 9–16. https://doi.org/10.1109/LRA.2021.3117245
7. E. Spyrakos-Papastavridis, J. S. Dai, Minimally model-based trajectory tracking and variable impedance control of flexible-joint robots, *IEEE Trans. Ind. Electron.*, **68** (2020), 6031–6041. https://doi.org/10.1109/TIE.2020.2994886
8. N. Kashiri, J. Lee, N. G. Tsagarakis, M. Van Damme, B. Vanderborght, D. G. Caldwell, Proxy-based position control of manipulators with passive compliant actuators: Stability analysis and experiments, *Rob. Auton. Syst.*, **75** (2016), 398–408. https://doi.org/10.1016/j.robot.2015.09.003
9. M. W. Spong, Modeling and control of elastic joint robots, *J. Dyn. Sys., Meas. Control.*, **109** (1987), 310–318. https://doi.org/10.1115/1.3143860
10. M. W. Spong, Adaptive control of flexible joint manipulators: Comments on two papers, *Automatica*, **31** (1995), 585–590. https://doi.org/10.1016/0005-1098(95)98487-Q
11. F. Ghorbel, J. Y. Hung, M. W. Spong, Adaptive control of flexible-joint manipulators, *IEEE Control Syst. Mag.*, **9** (1989), 9–13. https://doi.org/10.1109/37.41450
12. Y. Z. Chang, R. W. Daniel, On the adaptive control of flexible joint robots, *Automatica*, **28** (1992), 969–974. https://doi.org/10.1016/0005-1098(92)90149-A

13. M. Hong, X. Gu, L. Liu, Y. Guo, Finite time extended state observer based nonsingular fast terminal sliding mode control of flexible-joint manipulators with unknown disturbance. *J. Franklin Inst.*, **360** (2023), 18–37. https://doi.org/10.1016/j.jfranklin.2022.10.028
14. D. P. Nam, P. T. Loc, N. V. Huong, D. T. Tan, A finite-time sliding mode controller design for flexible joint manipulator systems based on disturbance observer, *Int. J. Mech. Eng. Rob. Res.*, **8** (2019), 619–625. https://doi.org/10.18178/ijmerr.8.4.619-625
15. J. W. Huang, J. S. Lin, Backstepping control design of a single-link flexible robotic manipulator, *IFAC Proceed. Vol.*, **41** (2008), 11775–11780. https://doi.org/10.3182/20080706-5-KR-1001.01994
16. X. Cheng, Y. Zhang, H. Liu, D. Wollherr, M. Buss, Adaptive neural backstepping control for flexible-joint robot manipulator with bounded torque inputs, *Neurocomputing*, **458** (2021), 70–86. https://doi.org/10.1016/j.neucom.2021.06.013
17. U. K. Sahu, B. Subudhi, D. Patra, Sampled-data extended state observer-based backstepping control of two-link flexible manipulator, *Trans. Inst. Measure. Control*, **41** (2019), 3581–3599. https://doi.org/10.1177/0142331219832954
18. J. Han, From PID to active disturbance rejection control, *IEEE Trans. Ind. Electron.*, **56** (2009), 900–906. https://doi.org/10.1109/TIE.2008.2011621
19. Y. Yan, L. Ding, Y. Yang, F. Liu, Discrete sliding mode control design for bilateral teleoperation system via adaptive extended state observer, *Sensors*, **20** (2020), 5091. https://doi.org/10.3390/s20185091
20. Y. Xia, M. Fu, C. Li, F. Pu, Y. Xu, Active disturbance rejection control for active suspension system of tracked vehicles with gun, *IEEE Trans. Ind. Electron.,* **65** (2018), 4051–4060. https://doi.org/10.1109/TIE.2017.2772182
21. A. A. Najm, I. K. Ibraheem, A. T. Azar, A. J. Humaidi, On the stabilization of 6-DOF UAV quadrotor system using modified active disturbance rejection control, in *Unmanned Aerial Systems*, (2021), 257–287. https://doi.org/10.1016/B978-0-12-820276-0.00018-2
22. X. Zhou, Q. Liu, Y. Ma, B. Xie, DC-link voltage research of photovoltaic grid-connected inverter using improved active disturbance rejection control, *IEEE Access*, **9** (2021), 9884–9894. https://doi.org/10.1109/ACCESS.2021.3050191
23. M. Li, J. Zhao, Y. Hu, Z. Wang, Active disturbance rejection position servo control of PMSLM based on reduced-order extended state observer, *Chin. J. Electr. Eng.*, **6** (2020), 30–41. https://doi.org/10.23919/CJEE.2020.000009
24. Z. L. Zhao, B. Z. Guo, A nonlinear extended state observer based on fractional power functions, *Automatica*, **81** (2017), 286–296. https://doi.org/10.1016/j.automatica.2017.03.002
25. D. Mu, L. Li, G. Wang, Y. Fan, Y. Zhao, X. Sun, State constrained control strategy for unmanned surface vehicle trajectory tracking based on improved barrier Lyapunov function, *Ocean Eng.*, **277** (2023), 114276. https://doi.org/10.1016/j.oceaneng.2023.114276
26. C. Wang, Y. Wu, J. Yu, Barrier Lyapunov functions-based adaptive control for nonlinear pure-feedback systems with time-varying full state constraints, *Int. J. Control Autom. Syst.*, **15** (2017), 2714–2722. https://doi.org/10.1007/s12555-016-0321-2
27. J. Li, Y. J. Liu, Control of nonlinear systems with full state constraints using integral Barrier Lyapunov Functionals, in *2015 International Conference on Informative and Cybernetics for Computational Social Systems (ICCSS)*, 2015, 66–71. https://doi.org/10.1109/ICCSS.2015.7281151

28. S. Zhang, M. Lei, Y. Dong, W. He, Adaptive neural network control of coordinated robotic manipulators with output constraint, *IET Control Theory Appl.*, **10** (2016), 2271–2278. https://doi.org/10.1049/iet-cta.2016.0009
29. X. Yu, W. He, H. Li, J. Sun, Adaptive fuzzy full-state and output-feedback control for uncertain robots with output constraint, *IEEE Trans. Syst. Man Cybern. Syst.*, **51** (2020), 6994–7007. https://doi.org/10.1109/TSMC.2019.2963072

AIMS Press